High Resolution Ultrasound Elastomicroscopy Imaging of Soft Tissues: System Development and Feasibility

Zheng YP[1], Bridal SL[2], Shi J[1], Saied A[2], Lu MH[1], Jaffre B[2], Mak AFT[1], and Laugier P[2],

[1] Rehabilitation Engineering Center, The Hong Kong Polytechnic University

[2] Laboratoire d'Imagerie Paramétrique, UMR CNRS 7623 – University of Paris VI

Short Title : **Ultrasound Elastomicroscopy**

Corresponding Author: YongPing ZHENG
Rehabilitation Engineering Center
The Hong Kong Polytechnic University
Kowloon, Hong Kong
Tel: 852 27667664
Fax: 852 23624365
Email: ypzheng@ieee.org

Submitted to: Physics in Medicine and Biology
1st submission: Jan 5 2004
Revision: Jun 13 2004

High Resolution Ultrasound Elastomicroscopy Imaging of Soft Tissues: System Development and Feasibility

Zheng YP[1], Bridal SL[2], Shi J[1], Saied A[2], Lu MH[1], Jaffre B[2], Mak AFT[1], Laugier P[2],
[1] Rehabilitation Engineering Center, The Hong Kong Polytechnic University
[2] Laboratoire d'Imagerie Paramétrique, UMR CNRS 7623 – University of Paris VI

ABSTRACT

Research in elasticity imaging typically relies on 1 to 10 MHz ultrasound. Elasticity imaging at these frequencies can provide strain maps with a resolution in the order of millimeters, but this is not sufficient for applications to skin, articular cartilage, or other fine structures. We developed a prototype high resolution elastomicroscopy system consisting of a 50 MHz ultrasound backscatter microscope system and a calibrated compression device using a load cell to measure the pressure applied on the specimen, which was installed between a rigidly fixed face-plate and a specimen platform. Radiofrequency data were acquired in a B-scan format (10 mm wide by 3 mm deep) in specimens of mouse skin and bovine patellar cartilage. The scanning resolution along the B-scan plane direction was 50 μm, and the ultrasound signals were digitized at 500 MHz to achieve a sensitivity of better than 1 μm for the axial displacement measurement. Because of elevated attenuation of ultrasound at high frequencies, special consideration was necessary to design a face-plate permitting efficient ultrasound transmission into the specimen and relative uniformity of the compression. Best results were obtained using a thin plastic film to cover a specially shaped slit in the face-plate. Local tissue strain maps were constructed by applying a cross-correlation tracking method to signals obtained at the same site at different compression levels. The speed of sound in the tissue specimen (1589.8 ± 7.8 m/s for cartilage and 1532.4 ± 4.4 m/s for skin) was simultaneously measured during the compression test. Preliminary results demonstrated that this ultrasound elastomicroscopy technique was able to map deformations of the skin and articular cartilage specimens to high resolution, in the order of 50 μm. This system can also be potentially used for the assessment of other biological tissues, bioengineered tissues or biomaterials with fine structures.

1. INTRODUCTION

Research in ultrasonic elasticity imaging typically relies on 1 to 10 MHz ultrasound which is the frequency range used for most medical imaging applications (Ophir et al. 1991). The spatial resolution obtained at these frequencies (on the order of millimeters) is not sufficient for the study of very fine structures in tissues such as skin layers or articular cartilage (Foster et al. 2000, Cohn et al. 1997a, 1997b, Fortin et al. 2003, Allan et al. 2002).

Nanoindentation (Pethica et al. 1983) has recently been used for the microscopic mechanical assessment of biological tissues including bone (Hengsberger et al. 2003), spinal fusion (Guo et al. 2001), calcified articular cartilage (Ferguson et al. 2003), and fresh articular cartilage (Hu et al. 2001). However, nanoindentation can not provide mechanical properties of tissues at different depths. The testing results are highly dependent on the surface condition of the specimen (Guo et al. 2001). Optical methods have recently been reported for the study of the mechanical properties and mechanotransduction of chondrocytes and the cell matrix of articular cartilage using compression, stretching, or osmotic swelling tests (Guilak et al. 1995, Schinagl et al. 1996, Setton et al. 1998, Narmoneva et al. 2001, Chen et al. 2001, Wang et al. 2002, Elliott et al. 2002, Flahiff et al. 2002). These optical methods required specimens to be well prepared for optical markers, and only the cut surface can be imaged. Elasticity imaging based on optical coherence tomography (OCT) has also been reported (Huang et al. 1991, Schmitt 1999). Optical beams are used to probe tissues at different depths, thus images of the scattering intensity from sub-surface structures of soft tissues are obtained to construct strain images (Schmitt 1998, Bao et al. 2002).

High-frequency (20 to 100 MHz) B-mode imaging (ultrasound biomicroscopy) has been widely used in recent years for the assessment of eye tissues, skin, blood vessel, and articular cartilage with an axial resolution of approximately 100 to 20 μm (Foster et al. 2000). Ultrasound biomicroscopy has been widely used for high frequency imaging of parameters related to tissue reflection, scattering and attenuation (Lizzi et al. 1987, Saied et al. 1997, Bridal et al. 1997). Such parameters are related to the material properties of the tissues and can be used for the detection of tissue modifications due to pathology or during therapy.

Elastography of artery walls has been reported using intravascular ultrasound backscattered signals (~30 MHz) obtained while cyclic blood pressure applied a temporally varying loading source on the vessel (de Korte et al. 1997, 2002). In other tissues, requiring an external compression

source, attempts have been made to acquire high frequency (50 MHz) ultrasound signals while squeezing tissue through a slit (2.6mm in width) in a compressor (Cohn et al. 1997a, b). However, use of the slit introduces important uncertainties in the mechanical boundary conditions on the specimen. Fortin et al. (2003) used two parallel plates to compress the two sides of cartilage specimens and to collect 50 MHz ultrasound from the open side. Using this configuration, the lateral tissue displacements in one direction were mapped under an axial compression. Based on the ultrasound indentation technique (Zheng and Mak 1996, 1999, Suh et al. 2001, Laasanen et al. 2002) using a probe with an in-series ultrasound transducer (frequency ranged from 5 to 15 MHz) and a load sensor, Zheng and coworkers have developed a number of systems for ,mapping one-dimensional mechanical properties of articular cartilage (AC) using high frequency ultrasound (20 to 50 MHz) (Zheng et al. 1998, 2001, 2002, 2003). The 2D high-frequency ultrasound elastography using axial compression has only been described in theory or using computer simulation in the literature (Konofagou et al. 2001, Righetti et al. 2002, 2003). In this paper, we introduce a 2D ultrasound elastomicroscopy system, which consists of a calibrated compressive device and a scanning ultrasound microscopy system (50 MHz), to achieve high-resolution elastography by applying uniform axial compression. Characteristics of the prototype system and preliminary results for AC and skin specimens are reported.

To demonstrate the feasibility of the ultrasound elastomicroscopy system, skin and articular cartilage specimens were tested in this study. The penetration depth and the focal zone of the 50MHz focused ultrasound beam match the thickness of skin and articular cartilage, which is approximately 1 to 2 mm. The layered mechanical properties of skin have been widely studied using various methods including ultrasound biomicroscopy (Foster et al. 2000). If the ultrasound elastomicroscopy can ultimately be applied in vivo, one potential application is to assess various diseases of skin, such as malignant melanoma (Foster et al. 2000) and basal cell carcinoma (Allan et al. 2002). The microstructure of skin matches well to the resolution of ultrasound biomicroscopy (Cohn et al. 1997b, Allan et al. 2002). AC is a biological weight-bearing tissue covering the ends of articulating bones within synovial joints. Because of its spatial variations of the water content, the proteoglycan concentration, and the orientation of the collagen fibrils, the mechanical properties of the AC are different at different depths (Mankin et al. 1994). The zonal variations of the tensile properties of AC have been conventionally characterized using carefully excised tissue slices and

optical methods (e.g. Woo et al. 1976, Chen et al. 2001). Such information may not only be important to understand the degeneration of AC but also to conduct tissue engineering of AC.

2. MATERIALS AND METHODS

2.1 Specimen Preparation

Fresh mature bovine patellae (n = 2) without obvious lesions were obtained from a local market. Osteochondral cylinders were cored out from the flat area of each patella AC using a metal punch with a diameter of 6.35 mm (1/4 inch). An AC specimen with a bone layer approximately 0.1~0.2 mm thick was prepared from the cylinders using a low speed diamond saw to cut away the bulk of the bone (Zheng et al. 2002). In comparison with the average AC thickness of approximately 1.5 mm, this bone layer was quite thin. This thin layer of bone was oriented towards the slit in the specimen platform during compression tests to prevent the soft cartilage tissue from being squeezed into the hole or slit while providing a passage for the focused high frequency ultrasound beam. The results of these AC specimens were used to demonstrate the feasibility of measuring in situ 2D depth-dependent elastic properties using the system developed in this work.

The fresh skin specimens (n = 1) used in this study were from a 4 week-old nude mouse (Rj:NMRI-nu (nu/nu), Elevage Janvier, Le Genest St Isle, France). The nude mouse model has been widely used in the study of tumors, as it is immunodeficient, and thus does not reject tumor transplantations from human (Maingonnat et al. 2003). Its nude feature also makes it easier to couple the ultrasound beam into its skin. Following sacrifice of the mouse, a transverse incision was opened from the stomach to the back. Specimens of skin (approximately 1.2 mm thick, 20 mm long by 10 mm wide) were obtained from the ventral, lateral and dorsal regions. These specimens provided a test medium with more homogeneous echogenicity than the AC and with no rigid bone layer.

2.2 Ultrasound Elastomicroscopy System and Data Acquisition

The ultrasound elastomicroscopy system consisted of a compression system and a backscatter ultrasound biomicroscope system. As shown in Figure 1, the specimen platform, in-series with a

load cell (25 N, Model ELFS-T3, Entran Devices, Inc., US) on its bottom, could be manually moved up and down. The specimen was installed on the top of the specimen platform, and covered by a rigidly fixed plate. As the specimen was pressed against the plate, the load applied on the specimen was measured by the load cell, which had been previously calibrated by placing different weights on the specimen platform. The ultrasound biomicroscope system consisted of a focused broadband polymer (PVDF) ultrasound transducer with a nominal frequency of 50 MHz (PI 50-2, Panametrics, US) and a broadband ultrasound pulser/receiver (5052PRX, Panametrics, US). The ultrasound beam was perpendicular to the specimen and compressor surfaces and centered with respect to the width of a specially cut, 1-mm wide by 12-mm long, slit in the compressing plate and focused within the region of the tissue to be imaged. Test data were acquired without any specimen present to insure that the slit did not significantly interfere with the passage of the ultrasound beam. The focal length of the transducer was 12.7 mm, and the diameter of the active element of this transducer was 6.35 mm. Therefore, the f-number (focal length/crystal diameter) was 2. The measured central frequency at the focus was 35 MHz, and its -6 dB bandwidth was 22 MHz. The lateral dimension of the focal zone of the ultrasound beam was determined using a fine wire with a diameter of 56 ± 0.8 μm (mean ± SD of 5 measurements using a micrometer). The wire was placed in a water tank and oriented normal to the sound beam direction and was scanned across the acoustic field using a computer-controlled 3D translating device (Parker Hannifin Corporation, Irvine, CA, USA) with a positional accuracy of 1 μm. The lateral acoustic pressure distribution in the focal plane was determined by the amplitudes of the received ultrasound signals as a function of the off-axis lateral distance in the geometrical focal plane (Raum and O'Brien 1997). To measure the axial dimension of the focal zone, a flat plane parallel to the acoustic beam axis was used and the transducer was vertically translated. The axial acoustic pressure distribution was determined by the amplitudes of the received ultrasound signals as a function of the axial distance (Schneider and Shung 1996). The measured -6 dB focal zone was 0.08 mm in diameter and 0.95 mm in axial length. A custom-built computer-controlled stepper-motor system (Sofratest, Ecquevilly, France) allowed the movement of the transducer in 50 μm steps along the length of the slit. The scan began approximately 2 mm beyond one lateral edge of the specimen and continued across the specimen up to 2 mm beyond the opposite edge. At each compression level and scan site, the backscattered radio frequency signal was digitized at 500 MHz and 8 bits using a digital oscilloscope (9350AL, LeCroy) and transferred

to a computer for off-line processing. After a scan was completed at one compression level, the specimen platform was moved upwards to compress the tissue specimen further, and a 15 min delay was respected before continuing data acquisition to allow the AC and skin tissues to achieve equilibrium states. The overall tissue compression was monitored using the change in the time of flight (TOF) between the echoes at the specimen surface and at the compressing platform beneath the specimen combined with information on the average speed of sound (obtained as described in the following section).

The repeatability of the scanning was tested by repeating scans without changing the compression level to ensure that the transducer returned to the same positions between consecutive scans. Different methods were investigated to find out how to best reduce uneven compression artifacts due to the presence of the compressor-plate slit. Measurements obtained with a thin bone layer on the upper side of the prepared AC specimen were compared with those with the non-rigid articulating surface of the cartilage against the compression slit. For the skin specimen, the measurements obtained with and without a thin film (approximately 0.1 mm in thickness) covering the slit were compared.

2.3 Calculation of Speed of Sound and Tissue Displacement

Figures 2a and 2b show two typical ultrasound images of a bovine AC specimen constructed from RF signals under two different compression levels. The grey levels of the image linearly represent the amplitude of the RF singles, i.e. uniform grey level (128) is baseline while black (0) and white (255) are maximum negative and maximum positive amplitude in the recorded range, respectively. Strong echoes from the thin bone layer can be seen at the tops of the images. Since the vertical coordinate of the images has not been scaled from time to distance in Figure 2, axial distances in figures 2a and 2b are displayed on the same time scale but cannot yet be compared in terms of distance.

Figures 2c and 2d show the A-mode ultrasound signals at the positions indicated by the dotted and solid lines, respectively, in Figures 2a and 2b. The dotted lines were located at a position without the presence of the specimen. A cross-correlation algorithm was used to track the movements of the selected echoes during compression (Zheng et al. 2002). The number, position

and width of the tracking windows (Figures 2c and 2d) could be freely adjusted. At each compression level, the TOF between the echoes from the platform at a site not covered by the specimen and from the specimen surface contacting the slit (T_3 and T_{3a} on Figure 3, before and after compression respectively) was used to calculate the distance between the slit/sample interface and the platform using the pre-measured speed of sound in the normal saline at room temperature (19.5 ± 1°C, c_{saline} = 1520 m/s). Assuming that the speed of sound in the soft tissue does not change after a small compression (this assumption would be further discussed later), it can then be calculated as:

$$c = c_{saline} \frac{(T_3 - T_{3a})}{T_0 - T_{0a}} \qquad (1)$$

where T_0 and T_{0a} are the TOF from the upper surface to the specimen/platform interface, before and after the compression, respectively. The measurement for T_0 and T_{0a} was made at three sites equally distributed along the specimen, and the averaged speed of sound was reported. Using this method, the speed of sound in the soft tissue can be measured precisely in-situ without the need for measuring the tissue thickness. A similar approach for the measurement of speeds of sound in tissue has been previously reported using indentation (Suh et al. 2001). Once the speed of sound was estimated for a specimen, time measurements were scaled to distances so that echo-tracking could be achieved in units of distance.

Tracking of ultrasound echoes scattered from the tissue at different depths was used to measure the local displacement of the tissue at that depth during the compression. The auto-segmentation and displacement measurement were applied line by line for the selected region of the RF image. Displacement calculation using the cross-correlation algorithm was applied for each 0.05 mm segment along for each A-line signal. The ROI (6.2 mm in width and 1.0 mm in height) was segmented into 50 portions for each of the 124 A-lines (0.05 mm interval) in the horizontal direction (with 60% overlap between adjacent segments) and the displacement from each interval and each A-line set was mapped to the displacement image. The local strains of the tissues at intermediate depths were then calculated from the displacements of the tissue at two adjacent depths. A strain image was formed from the local strain profiles along each ultrasound signal. The grey levels of the strain image indicate the local strain values.

3. RESULTS

Scanning was repeatable as demonstrated by the high correlation of radio frequency signals obtained from the same site during different scans ($R^2 > 0.97$). Progressive compressions could be applied smoothly to the specimen using the compression system. It was verified that the side-lobe echoes originating from the passage of the sound beam through the slit were considerably smaller than the echoes from structures in the AC (< -26 dB) and skin (< -46 dB) tissues. Figure 4 shows the RF ultrasound image obtained by scanning across the middle portion of the slit (in a direction perpendicular to the long axis of the slit) without the specimen installed. The pulser/receiver was set to achieve the maximum sensitivity for the AC specimens. The dotted line in the middle of Figure 4a indicates where the RF signals in Figure 4b was obtained. The scanning along the long axis of the slit for the specimen measurement was conducted at this position.

More uniform compressions were obtained when the overlying thin bone layer was placed at the interface with the compressor-plate slit than when cartilage tissue without bone layer was placed. Figure 5 shows two B-mode ultrasound images of an AC specimen with a thin layer of bone at the interface of the AC and the slit. After an overall deformation of 16%±1% (mean±SD of three measurements at positions 1 mm apart in the central region of the specimen) was applied, the AC layer was compressed as observed in Figure 5b. The displacement of the bone layer was 5.1%±0.7% of the overall deformation of the specimen. Figure 6 shows images obtained from the same specimen, but with the bone interface turned toward the compressing platform so that the AC surface was directly in contact with the slit. After the same amount of deformation (16%±2%) was applied, the AC tissues at the top region were squeezed into the slit as observed in Figure 6b. The displacement of the upper cartilage surface was 67%±1% of the overall deformation of the specimen. Because of this squeezing effect, the stresses inside the AC tissues could not be uniformly distributed, and strain images would not only be influenced by the compression level but also be affected by the interaction between the AC tissues and the slit. It was noted that the scattering ultrasound signals obtained with the bone layer contacting the slit were weaker than those obtained without the bone layer. Therefore, it is important to prepare AC specimens with suitable thickness of bone layers to prevent the tissue from being squeezed into the slit while minimizing attenuation as

much as possible.

Similar results were obtained from the skin specimen. Only very slight movement of the upper surface of the skin specimen (2.8%±1%) could be observed in comparison with the case with no film used (92%±5%) when a deformation of approximately 35% was applied. The displacements of the skin tissue caused by the squeezing was almost the same as the overall deformation applied on the tissue in the case without the film. The film successfully prevented squeezing of the skin tissue into the slit and provided a sufficiently transparent acoustic window to maintain exploitable echoes across the skin's depth. However, it was noted that the same film could not prevent squeezing of the AC tissues using a similar configuration.

For the tests on the AC and skin specimens, the speed of sound in the specimens were measured using the method described by Equation 1. For the AC specimen as shown in Figure 5, the mean speed in the AC specimen was 1589.8 ± 7.8 m/s, after 5 steps of compression (21.5 kPa). With 12 compression steps (2.1 kPa), the calculated mean speed in the skin specimen was 1532.4 ± 4.4 m/s. It was noted that the speeds of sound in both tissue specimens tended to increase slightly as the increase of the pressure when the deformation was large enough. However, more specimens would be required to better understand the stress-dependence of the speeds of sound in soft tissues. The root-mean-square difference of the speed of sound measured for the compression steps of approximately 5% was smaller than 1.3% for the specimens tested in this study. The result showed that the assumption of a constant speed of sound for each compression step was acceptable in using Equation 1.

Figure 7 shows the preliminary results of 2D ultrasound elastomicroscopy in an AC specimen. A B-mode ultrasound image constructed with RF signals collected from an AC specimen is shown in Figure 7a that corresponds to the B-mode image shown in Figure 5a. Figure 7b shows an image formed by the tissue displacement within the region of interest (ROI) outlined by the dashed rectangle in Figure 7a. The local strain of the tissue represented by each segment of each A-line ultrasound signal was further derived and a local strain image was formed (Figure 7c). The strains were induced by a step of an overall compression of 0.042 mm applied to the specimen which had already been deformed before this additional compression (the mean stress was increased from 17.4 kPa to 24.1 kPa). The grey level in Figure 7c indicates the value of strain. Brighter pixels

in the lower potion of the image (near the AC/platform interface, i.e. the superficial potion of AC) indicate that larger strain occurred near the articular surface in comparison with zones near the bone layer. This finding agrees with the results of the 1D transient measurement previously reported (Zheng et al. 2002). Some noise could be observed in the preliminary results of strain image as shown in Figure 7c. This issue was further discussed in the discussion section.

4. DISCUSSION

Elastographic measurements could potentially be combined with ultrasound biomicroscopy to provide complementary high-resolution information linked to material stiffness and other mechanical parameters. Though the concept seems straightforward, developing an experimental setup to load a specimen while collecting high-frequency ultrasound signals along the same direction remains a challenge. Due to the lack of high-frequency multi-element ultrasound arrays, multi-dimensional high-frequency ultrasound signals must be collected by scanning a focused transducer above the tissue specimen. The measurement or imaging of tissue elasticity using ultrasound elastography involves compressing the tissue and collecting ultrasound signals simultaneously in the compression direction. Because of elevated attenuation of ultrasound at high frequencies, material placed between the scanning transducer and the compressed tissue must be kept to a minimum. In this study, we introduced an ultrasound elastomicroscopy system which could be used to compress small tissue specimens and simultaneously collect high frequency ultrasound signals in the compression direction. The focused ultrasound beam passed through a slit with a width of approximately 1 mm located in the middle of the compression plate. More uniform compressions were obtained using plastic film covering of the skin and the overlying thin bone layer of the cartilage than when these materials were not placed between the specimen and the compressing plate. Without the bone layer for AC or the film plate for the skin specimen, the deformed tissues were squeezed into the slit (67% and 92% of total deformation, respectively).

It was noted that the 50 MHz ultrasound was significantly attenuated after passing through the bone layer of AC. Thus, the bone layer thickness should be minimized as much as possible to increase the amplitude of ultrasound echoes scattered from the tissues inside the AC layer. On the other hand, a certain bone thickness was necessary to prevent compression of tissue into the slitted

compression plate. It was found that ultrasound signals scattered inside the AC layer could be detected throughout the entire depth for most specimens while the thin bone layer held the back surface of the AC in place. However, the preparation of a bone layer with suitable thickness for the AC specimen is time consuming. Several types of rigid plates with different thickness had also been tried to replace the bone layer for AC specimen. It was found that for tissues such as AC, which is stiffer than skin tissues, thin plastic films did not appear to be adequate while thick film could introduce strong interface echoes (including multiple reflections within the plate) which seriously overlapped with the relatively weak scattering signals from the AC tissues. Efforts are being continued to find alternatives to the bone interface for AC compression so as to save the time in preparing a uniform thin layer of bone for the AC specimen and to extend the technique for in-vivo assessment for AC where the bone side is not accessible.

The movement of ultrasound signals under compression was determined using a cross-correlation tracking method. The sensitivity of the displacement measurement depends on the sampling rate of the A/D converter. For the average speed of sound of 1590 m/s measured in this study for AC, the theoretical sensitivity of the displacement measurement was 1.59 μm for the 500 MHz sampling rate. Using a five times linear interpolation for the collected ultrasound echo trains in the time domain before the cross-correlation operation, the measurement sensitivity was improved to 0.32 μm (Ophir et al. 1999, Zheng 2001, 2002). This sensitivity for the displacement was adequate for the measurements in this study. According to their numerical simulation results, Righetti et al. (2002, 2003) reported that the lateral and axial resolution limits of the strain images obtained using ultrasound elastography were on the order of the sonographic lateral resolution and the ultrasonic wavelength, respectively. In the present system, they are 90 μm (measured experimentally) and 35 μm (calculated according to the central frequency of 35 MHz, -6 dB bandwidth of 22 MHz and the speed of sound of 1590 m/s in AC, Foster et al. 2000), respectively. Our preliminary experimental results demonstrated that a similar resolution could be achieved by the elastomicroscopy system. However, more systematic experiments using fine phantoms are required to further study the resolutions of the system.

The measured speed of sound for the bovine AC specimen (1590 m/s) was within the range reported in the literature, e.g. 1532 to 1754 m/s (Toyras et al. 2003). The speed of sound of the

mouse skin (1532 m/s) also agreed with value previously reported, e.g. 1510 to 1543 m/s (Bhagat et al. 1980). The speed of sound was assumed to be the same before and after each step of compression. This assumption should be reasonable for the relatively small deformation of 1.6%±0.9% for each compression used in this study (this value was obtained by averaging the deformation of each step of compression for the AC and skin specimens). If a larger deformation is applied, the shift of the echo due to the change of the speed of sound should be taken into account in the extraction of the displacement and strain images. The deformation-dependent speed of sound may induce a bias to the estimated displacement and strain values. In addition, it should be noted that the speed of sound measured using this method is an average value of the speeds of sound in the tissues. The speed of sound in articular cartilage has been reported to be depth-dependent (Patil et al. 2004). Since the stiffness of the cartilage tissues is depth-dependent as well (Schinagl et al. 1996, Zheng et al. 2001, 2002), the cartilage will be deformed non-uniformly under compression. A softer layer contributes more for a certain overall deformation. Hence, the speed of sound in the softer layer weights more in the calculation of the average value of the speed of sound in the cartilage. The depth-dependent property of the speed of sound can affect the computation of the displacement image. However, for the strain calculation, the speed of sound can be cancelled out if it is assumed not to be a function of strain for a small deformation (Zheng et al. 2001).

The preliminary results of strain images of the tissue specimens under compression have been reported. The regions with larger deformations in the AC specimen could be successfully differentiated from other regions, though the noise level in the strain image could be observed. The noise was possibly due to 1) no additional signal processing like low pass filter was used after the displacement and strain were derived using the cross-correlation algorithm; 2) de-correlation of the ultrasound signal occurred after the compression was made; 3) there was lateral movement of the tissue involved during the compression; and 4) the backscattering signals at some regions of the AC specimen was not large enough. We noted that ultrasound backscattering signals in AC were much smaller in comparison with other tissues like skin and muscle, particularly a thin bone layer was required to maintain proper boundary conditions during the compression. Since nondestructive mapping of the mechanical properties of AC in situ attracts great interests for the AC biomechanicists, we are continuing to develop new compression methods for AC and improved signal processing methods to achieve higher signal-to-noise ratio for the backscattering signals.

Overcoming the above challenges, the system introduced in this paper can also be potentially used for the assessment of other biological tissues, bioengineered tissues or biomaterials with fine structures. Local strain images can be combined with images of intrinsic material properties such as the ultrasonic backscatter or attenuation coefficients to provide complementary information related to changes in tissue structure. By improving the proposed method together with a real-time ultrasound biomicroscope and a hand-held probe, it is feasible to construct an ultrasound elastomicroscopy for in vivo assessment of soft tissues, like the skin. Further efforts are required to achieve a uniform compression for the tissues in vivo.

ACKNOWLEDGEMENTS

This work is partially supported by the France/Hong Kong Joint Research Scheme PROCORE (F-HK12/01T) and the Research Grant Council of Hong Kong (PolyU5199/02E, PolyU5245/03E). The authors would like to thank Erwan for his help in preparing the skin specimens.

REFERENCES

Allan E, Pye DA, Levine EL, and Moore JV. Non-invasive pulsed ultrasound quantification of the resolution of basal cell carcinomas after photodynamic therapy**.** Lasers in medical science.2002**;** 17: 230-237.

Bao XD, Zheng YP, Zhao J, and Xiao SJ. Estimation of deformation from OCT images based on multiresolution matching. Proceedings of the Conference on Biomedical Engineering BME2002, Hong Kong, pp. 61-64, 2002.

Bhagat PK, Kerrick W, and Ware RW. Ultrasonic characterization of aging in skin tissue. Ultrasound in medicine and biology 1980; 6: 369-375.

Bridal SL, Fornes P, Bruneval P and Berger G. Correlation of ultrasonic attenuation (30 to 50 MHz) and constituents of atherosclerotic plaque, Ultra Med Biol 1997; 23: 691-703.

Chen AC, Bae WC, Schinagl RM, and Sah RL. Depth- and strain-dependent mechanical and electromechanical properties of full-thickness bovine articular cartilage in confined compression. Journal of Biomechanics 2001; 34: 1-12.

Cherin E, Saied A, Pellaumail B, Loeuille D, Laugier P, Gillet P, Netter P, and Berger G. Assessment of rat articular cartilage maturation using 50-MHz quantitative ultrasonography. Osteoarthritis and Cartilage. 2001; 9: 178-186.

Cohn NA, Emelianov SY, Lubinski MA, and O'Donnell M. An elasticity microscope. Part I: Methods. IEEE Transactions on Ultrasonics, Ferroelectrics, and Frequency Control 1997a; 44: 1304-1319.

Cohn NA, Emelianov SY, and O'Donnell M. An elasticity microscope. Part II: Experimental Results, IEEE Transactions on Ultrasonics, Ferroelectrics, and Frequency Control 1997b; 44: 1320-1331.

deKorte CL, Cespedes EI, vanderSteen AFW, and Lancee CT. Intravascular elasticity imaging using ultrasound: Feasibility studies in phantoms. Ultrasound in Medicine and Biology 1997; 23: 735-746.

de Korte CL, and van der Steen AFW. Intravascular ultrasound elastography: an overview. Ultrasonics 2002; 40: 859-865.

Elliott DM, Narmoneva DA, and Setton LA. Direct measurement of the Poisson's ratio of human patella cartilage in tension. Journal of Biomechanical Engineering-Transactions of ASME 2002; 124: 223-228.

Ferguson VL, Bushby AJ, and Boyde A. Nanomechanical properties and mineral concentration in articular calcified cartilage and subchondral bone. Journal of Anatomy 2003; 203: 191-202.

Flahiff CM, Narmoneva DA, Huebner JL, Kraus VB, Guilak F, and Setton LA. Osmotic loading to determine the intrinsic material properties of guinea pig knee cartilage. Journal of Biomechanics 2002; 35: 1285-1290.

Fortin M, Buschmann MD, Bertrand MJ, Foster FS, Ophir J. Dynamic measurement of internal solid displacement in articular cartilage using ultrasound backscatter. Journal of Biomechanics 2003; 36: 443-447.

Foster FS, Pavlin CJ, Harasiewicz KA, Christopher DA, and Turnbull DH. Advances in ultrasound biomicroscopy. Ultrasound in Medicine and Biology 2000; 26: 1-27.

Guo LH, Guo X, Leng Y, Cheng JCY, and Zhang XD. Nanoindentation study of interfaces between calcium phosphate and bone in an animal spinal fusion model. Journal of Biomedical Materials Research 2001; 54: 554-559.

Guilak F, Ratcliffe A, Mow VC. Chondrocyte deformation and local tissue strain in AC: A confocal microscopy study. Journal of Orthopaedic Research 1995; 12: 410-422.

Hengsberger S, Enstroem J, Peyrin F, and Zysset Ph. How is the indentation modulus of bone tissue related to its macroscopic elastic response? A validation study. Journal of Biomechanics 2003; 36: 1503-1509.

Hu K, Radhakrishnan P, Patel RV, and Mao JJ. Regional structural and viscoelastic properties of fibrocartilage upon dynamic nanoindentation of the articular condyle. Journal of Structural Biology 2001; 136: 46-52.

Huang D, Swanson EA, Lin CP, Schuman JS, Stinson WG, Chang W, Hee MR, Flotte T, Gregory K, Puliafito CA, and Fujimoto JG. Optical coherence tomography. Science 1991; 254: 1178-1181.

Konofagou EE, Harrigan TP, Ophir J, Krouskop TA. Poroelastography: Imaging the poroelastic properties of tissues. Ultrasound in Medicine and Biology 2001; 27: 1387-1397.

Laasanen MS, Toyras J, Hirvonen J, Saarakkala S, Korhonen RK, Nieminen MT, Kiviranta I, Jurvelin JS. Novel mechano-acoustic technique and instrument for diagnosis of cartilage degeneration. Physiological Measurement 2002; 23: 491-503.

Lizzi FL, Ostromogilsky M, Feleppa EJ, Rorke MC and Yaremko MM. Relationship of ultrasonic spectral parameters to features of tissue microstructure, IEEE Trans UFFC 1987; 33: 319-329.

Maingonnat C, Courel MN, Bertrand P, Vincent JC, Sesbou R, and Delpech B. Hyaluronidase in sera of tumour-bearing nude mice. Biomarkers 2003; 8: 333-338.

Mankin HJ, Mow VC, Buckwalter JA, Iannotti JP, and Ratcliffe A. Form and function of articular cartilage. In: Simnon SR, ed. Orthopaedic Basic Science. American Academy of Orthopaedic Surgeons, 1994.

Narmoneva DA, Wang JY, and Setton LA. A noncontacting method for material property determination for articular cartilage from osmotic loading. Biophysical Journal 2001; 81: 3066-3076.

Ophir J, Cespedes I, Ponnekanti H, Yazdi Y, and Li X. Elastography: a quantitative method for imaging the elasticity of biological tissues. Ultrasonic Imaging 1991; 13: 111-134.

Ophir J, Alam SK, Garra B, Kallel F, Konofagou E, Krouskop T, and Varghese T. Elastography: ultrasonic estimation and imaging of the elastic properties of tissues. Proc Instn Mech Engrs 1999; 213 (Part H): 203-233.

Patil SG, Zheng YP, Wu JY, and Shi J. Measurement of depth-dependency and anisotropy of ultrasound speed of bovine articular cartilage in vitro. Ultrasound in Medicine and Biology. 2004. In print.

Pethica JB, Hutchings R, and Oliver WC. Hardness measurement at penetration depths as small as 20-nm. Philosophical Magazine A - Physics of Condensed Matter Structure Defects and Mechanical Properties 1983; 48: 593-606.

Raum K and O'Brien WD. Pulse-echo field distribution measurement technique for high frequency ultrasound sources. IEEE Trans. Ultrason., Ferroelec., Freq. Contr. 1997; 44: 810-815.

Righetti R, Ophir J, and Ktonas P. Axial resolution in elastography. Ultrasound in Medicine and Biology 2002; 28: 101-113.

Righetti R, Srinivasan S, and Ophir J. Lateral resolution in elastography. Ultrasound in Medicine and Biology 2003; 29: 695-704.

Saied A, Cherin E, Gaucher H, Laugier P, Gillet P, Floquet J, Netter P, and Berger G. Assessment of articular cartilage and subchondral bone: subtle and progressive changes in experimental osteoarthritis using 50 MHz echography in vitro. Journal of Bone and Mineral Research 1997; 12: 1378-1387.

Schinagl RM, Ting MK, Price JH, and Sah RL. Video microscopy to quantitate the inhomogeneous equilibrium strain within articular cartilage during confined compression. Annals of Biomedical Engineering 1996; 24: 500-512.

Schmitt JM. OCT elastography: Imaging microscopic deformation and strain of tissue. Optics Express 1998; 3: 199-211.

Schmitt JM. Optical coherence tomography (OCT): A review. IEEE Journal of Selected Topics in Quantum Electronics 1999; 5: 1205-1215.

Schneider B and Shung KK. Quantitative analysis of pulsed ultrasonic beam patterns using a Schileren system. IEEE transactions on ultrasonics, ferroelectrics, and frequency control. 1996; 43: 1181-1186.

Setton LA, Tohyama H, and Mow VC. Swelling and curling behaviors of articular cartilage. Journal of Biomechanical Engineering 1998; 120: 355-361.

Suh JKF, Youn I, and Fu FH. An in situ calibration of an ultrasound transducer: a potential application for an ultrasonic indentation test of articular cartilage. Journal of Biomechnics 2001; 34: 1347-1353.

Toyras J, Laasanen MS, Saarakkala S, Lammi MJ, Rieppo J, Kurkijarvi J, Lappalainen R, and Jurvelin JS. Speed of sound in normal and degenrated bovine articular cartilage. Ultrasund in Medicine and Biology 2003; 29: 447-454.

Wang CCB, Guo XE, Sun DN, Mow VC, Ateshian GA, Hung CT. The functional environment of chondrocytes within cartilage subjected to compressive loading: A theoretical and experimental approach. Biorheology Sp. Iss. 2002; 39: 11-25.

Woo SLY, Akeson WH, and Jemmott GF. Measurements of nonhomogeneous, directional mechanical properties of articular cartilage in tension. Journal of Biomechanics 1976; 9: 785-791.

Zheng YP and Mak AFT. An ultrasound indentation system for biomechanical properties assessment of soft tissues in vivo. IEEE Transactions on Biomedical Engineering 1996; 43: 912-918.

Zheng YP, Mak AFT, Qin L, and Ding CX. Ultrasound elastography of articular cartilage: A preliminary study. Proc 20th Annual International Conference of IEEE EMBS, Hong Kong, 1998: 1940-1942.

Zheng YP, Mak AFT. Extraction of quasilinear viscoelastic parameters for lower limb soft tissues from manual indentation experiment. ASME Transactions, Journal of Biomechanical Engineering 1999; 121: 330-339.

Zheng YP, Ding CX, Bai J, and Mak AFT. Measurement of nonhomogeneous compressive properties of trypsin treated articular cartilage: An ultrasound investigation. Medical and Biological Engineering and Computing 2001; 39: 534-541.

Zheng YP, Mak AFT, Lau KP, Qin L. An ultrasonic measurement for in vitro depth-dependent equilibrium strains of articular cartilage in compression. Physics in Medicine and Biology 2002; 47: 3165-3180.

Zheng YP, Bridal L, Shi J, Saied A, Lu MH, Jaffre B, Mak AFT, Laugier P, and Qin L. Ultrasound Elastomicroscopy for Articular Cartilage: From Static to Transient and 1D to 2D. SPIE Medical Imaging: Ultrasonic Imaging and Signal Processing Conference, February 15-20 2003, San Diego, USA. 2003; 398-410.

FIGURE CAPTIONS

Figure 1. (a) A cross-sectional view of the compression system used for the ultrasound elastomicroscopy. (b) Top view of the compressor with the slit (1 mm in width and 12 mm in length), specimen, loading plate and specimen platform being highlighted (not to scale). The specimen was installed between the loading plate and the platform, and load was applied from the bottom. The ultrasound transducer could be translated in 3D, and the specimen was scanned along the slit.

Figure 2. B-mode RF ultrasound images (10 mm in width and 3 mm in height) of a typical AC specimen (a) before and (b) after a compression (9.2 kPa) was applied. The ultrasound beam propagated along z direction. The grey levels of the image linearly represent the amplitude of the RF signals, i.e. uniform grey level (128) is baseline while black (0) and white (255) are maximum negative and maximum positive amplitude in the recorded range. RF signals in (c) and (d) correspond to the positions indicated by the dotted lines and solid lines, respectively, in (a) and (b). The pairs of horizontal dashed lines in (c) and (d) formed tracking windows to follow the movements of the corresponding ultrasound echoes. The signals in thin lines correspond to the selected echoes in the image (b), while the signals in bold lines within the tracking windows in (c) and (d) correspond to the image (a), i.e. before compression. The values beside the tracking windows indicate the correlation coefficients of the cross-correlation operations for the corresponding echoes before and after the compression was applied. The echo signals from the interfaces of saline/bone/AC and AC/platform were saturated in (d).

Figure 3. Schematic representation of the specimen (a) before and (b) after a compression and the ultrasound time-of-flight (TOF) involved in the calculation of the speed of sound in the specimen. T_1 and T_{1a} represent the TOF in the rigid layer (either the bone layer for AC or the film layer for skin)

before and after the compression; T_2 and T_{2a} represent the TOF in the soft tissue; T_3 and T_{3a} represent the TOF between the specimen upper surface and the surface of the specimen platform in saline.

Figure 4. (a) The RF ultrasound image (6 mm in width and 3 mm in height) obtained by scanning across the slit. The ultrasound beam propagated along z direction. The grey levels of the image linearly represent the amplitude of the RF signals, i.e. uniform grey level (128) is baseline while black (0) and white (255) are maximum negative and maximum positive amplitude in the recorded range. (b) The RF signal at the position indicated by the dotted line in (a). This position was at the middle of the slit. (c) Illustration showing the scanning direction. The arrow in (c) indicates the scanning direction to obtain the image shown in (a), and the dashed line indicates the scanning direction for the measurement of specimens. According to (a), the transparent acoustic window formed by the slit was approximately 0.8 mm in width.

Figure 5. B-mode ultrasound images of a bovine AC specimen (with a thin bone layer on the top) collected pre compression and post compression with a deformation of 16%±1% (mean±SD of three measurements at positions 1 mm apart in the central region of the specimen). During the compression, the bottom compressing platform was moved upwards, and the top compressing plate with the slit (not shown in the figure) was fixed. The ultrasound signals were collected with the 50 MHz ultrasound beam passing through the slit. In these two images and those in Figures 6, the envelopes of the RF signals were used to form images. The grey levels of the images represent the amplitude of the envelope signal, i.e. black (0) and white (255) are the 0 and maximum envelope amplitude in the recorded range, respectively.

Figure 6. B-mode ultrasound images of the bovine AC specimen (same as that shown in Figure 5)

collected pre and post compression with a deformation of 16%±2%. The thin bone layer was oriented towards the compressing platform at the bottom. Other procedures were the same as those described in Figure 5. It can be observed that the AC tissues were squeezed into the slit and moved upwards.

Figure 9. (a) A B-mode ultrasound image (10 mm in width and 3 mm in height) constructed with RF signals. The grey levels of the image linearly represent the amplitude of the RF signals, i.e. uniform grey level (128) is baseline while black (0) and white (255) are maximum negative and maximum positive amplitude in the recorded range. Two conjunctive frames of image (with a compression of 0.042 mm and average stress changed from 17.4 to 24.1 kPa) were used for the cross-correlation calculation. The dashed rectangle indicates the region of interest (ROI) for the displacement and strain images (6.2 mm in width and 1.0 mm in height). (b) The image formed by the local displacements within the ROI (50 segments for each of the 124 A-line signals). Brighter pixels in (b) represent larger tissue movements in the upward direction. (c) The corresponding local strain images of the ROI. Brighter pixels (c) represent larger strains in the upward direction. No filtering and smoothing was used in constructing the displacement and strain images as shown in (c) and (d).

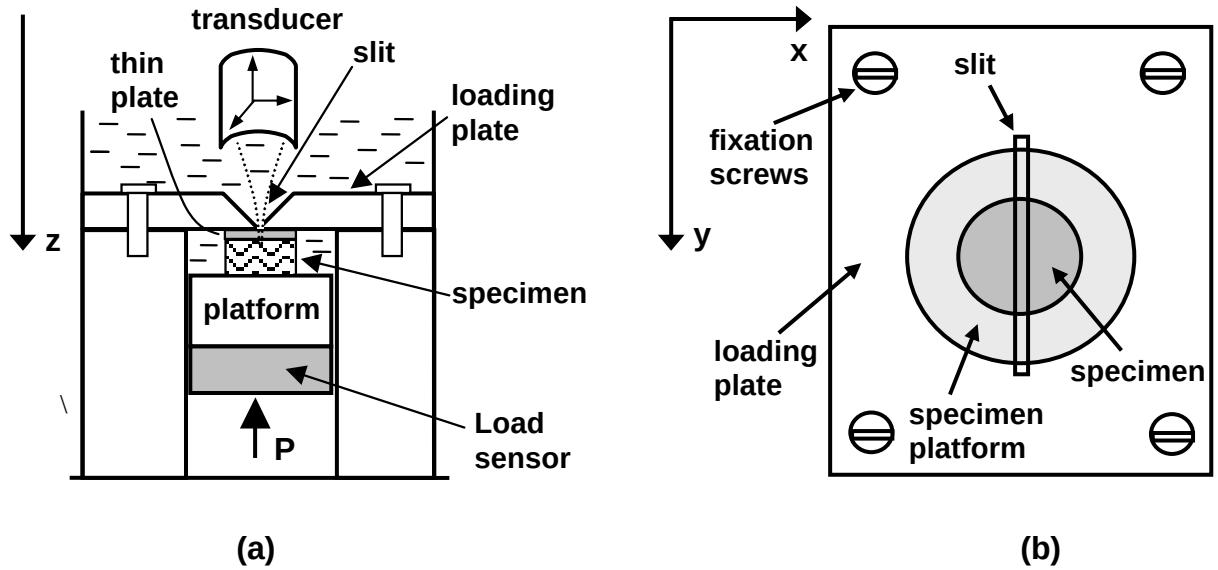
transducer
thin plate
slit
loading plate
z
specimen
platform
Load sensor
P
(a)
x
y
slit
fixation screws
loading plate
specimen
specimen platform
(b)

Figure 1

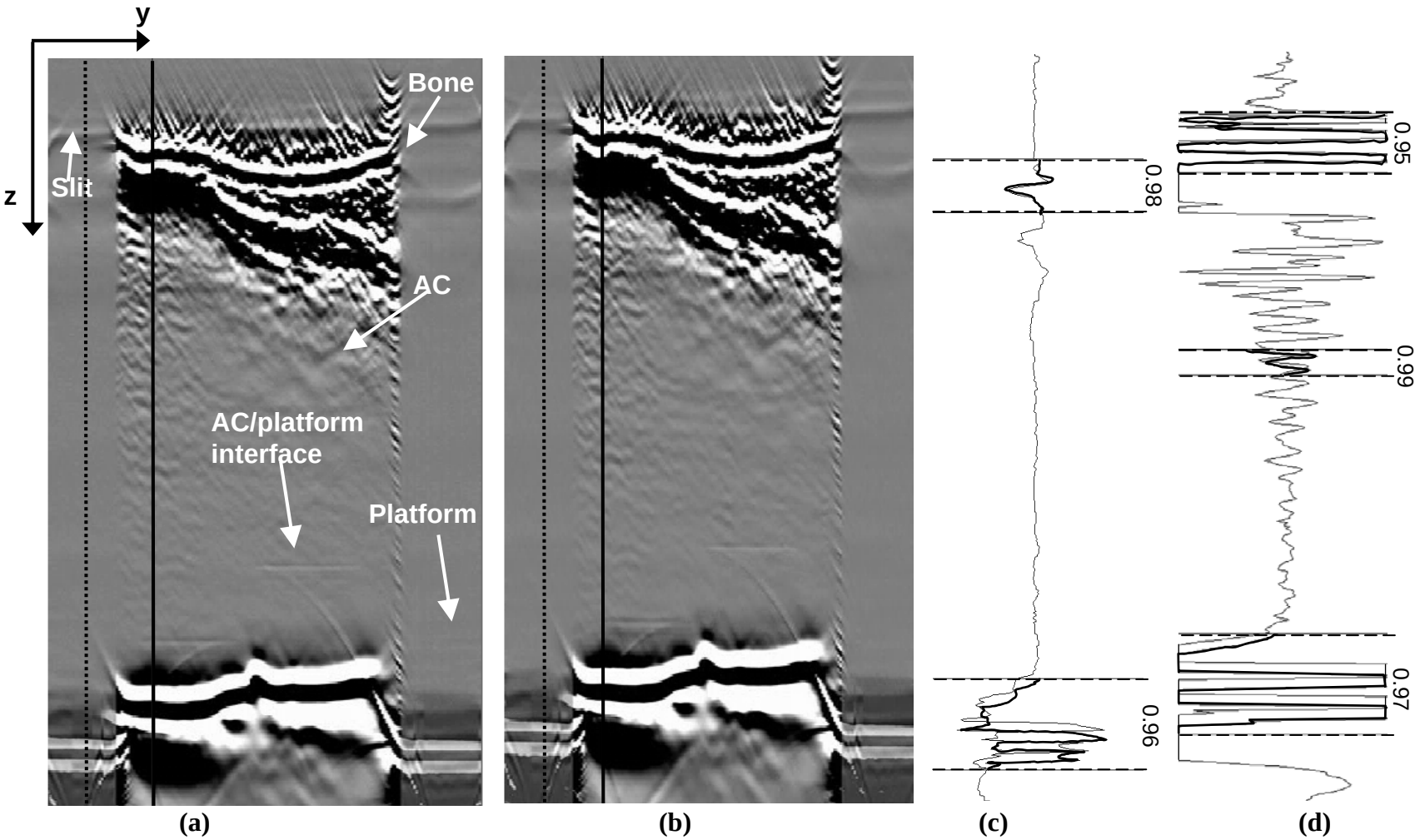
y
z
Slit
Bone
AC
AC/platform
interface
Platform
0.98
0.96
0.95
0.99
0.97
(a)
(b)
(c)
(d)

Figure 2

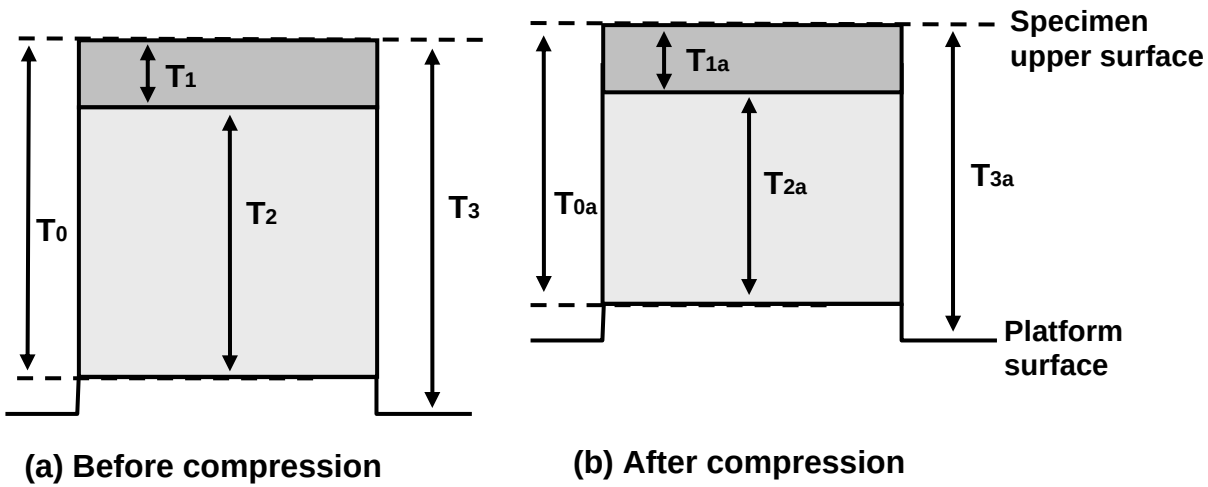
T1
T0
T2
T3
T1a
T0a
T2a
T3a
Specimen
upper surface
Platform
surface
(a) Before compression
(b) After compression

Figure 3

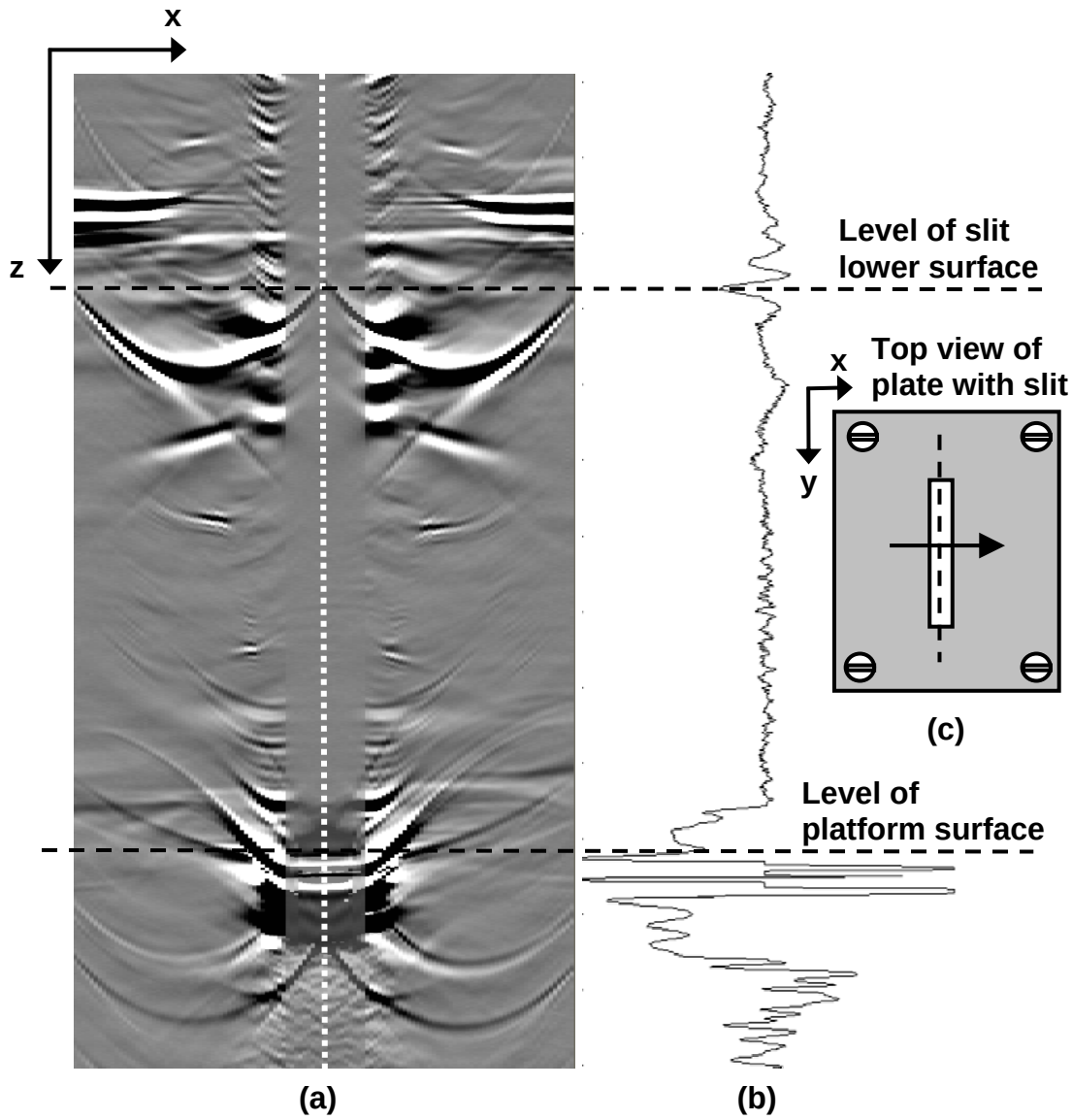
x
z
Level of slit
lower surface
x
Top view of
plate with slit
y
(c)
Level of
platform surface
(a)
(b)

Figure 4

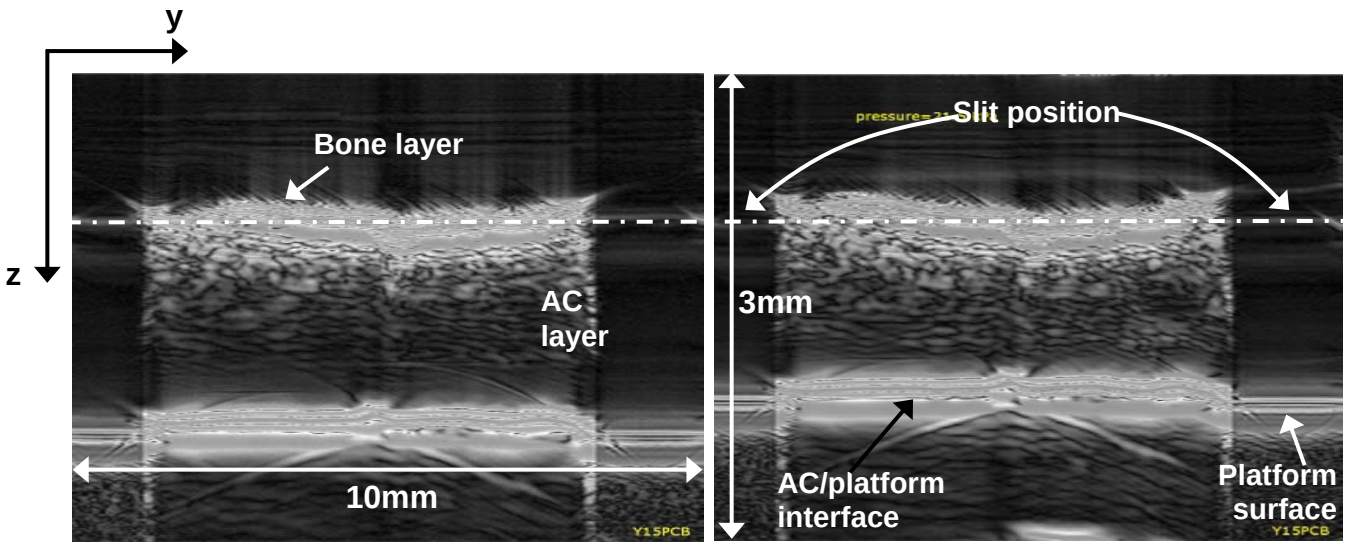

(a) Pre compression **(b) Post compression (16%)**

Figure 5

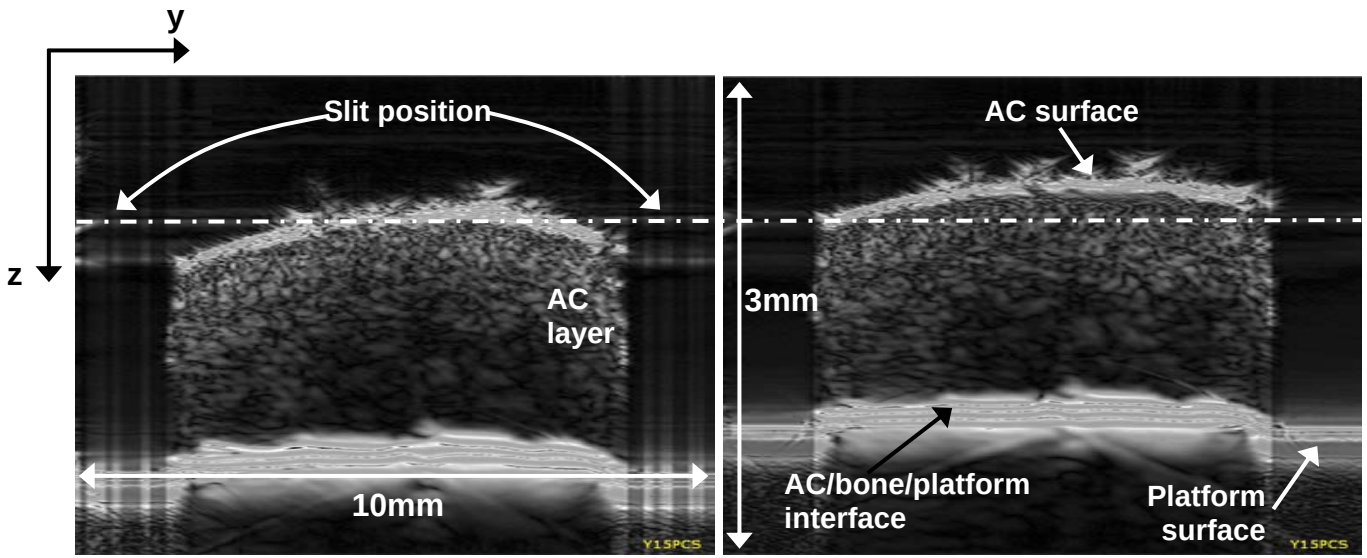
y
z
Slit position
AC
layer
10mm
AC surface
3mm
AC/bone/platform
interface
Platform
surface
(a) Pre compression
(b) Post compression (16%)

Figure 6

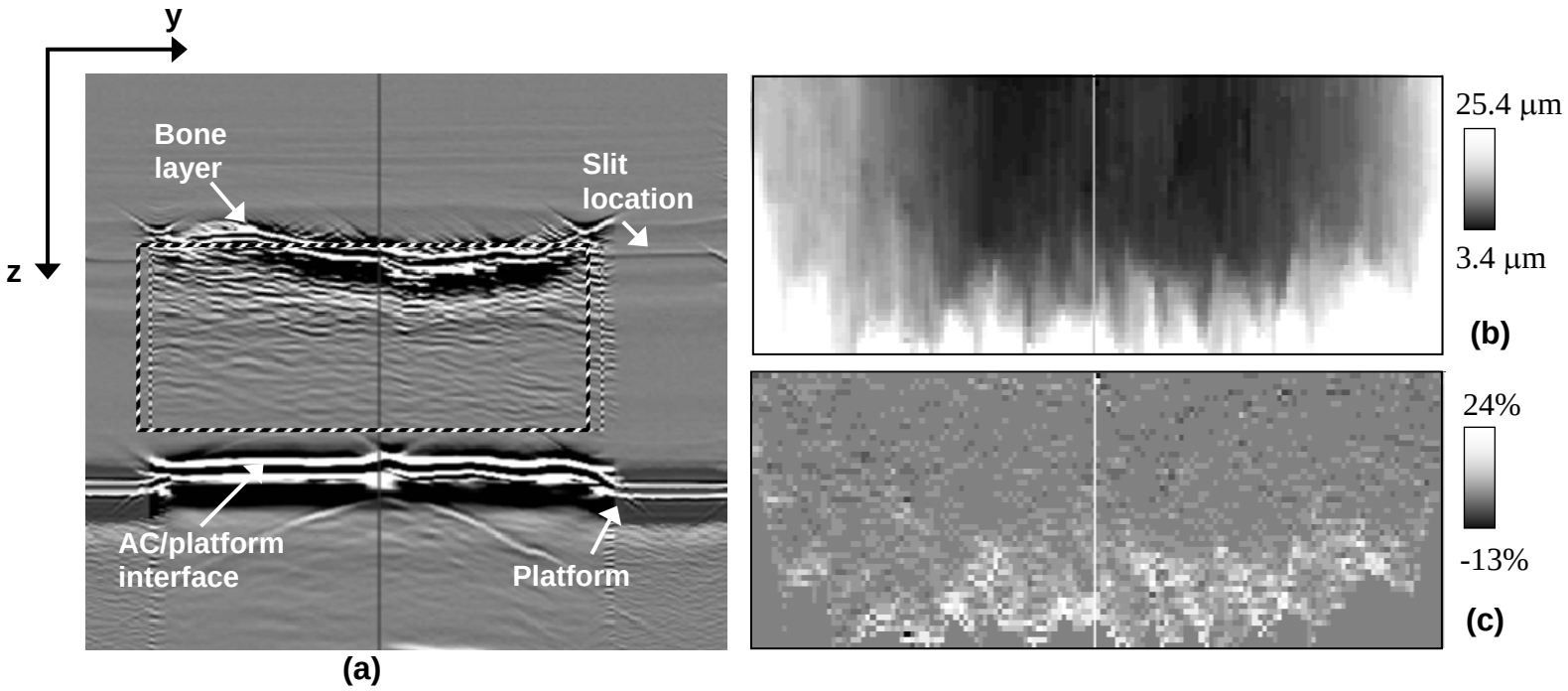
y
z
Bone layer
Slit location
AC/platform interface
Platform
(a)
25.4 μm
3.4 μm
(b)
24%
-13%
(c)

Figure 7